Published in final edited form as:
Magn Reson Med. 2010 November ; 64(5): 1453–1460. doi:10.1002/mrm.22543.

Rotating Frame Spin Lattice Relaxation in a Swine Model of Chronic, Left Ventricular Myocardial Infarction

Walter RT Witschey, PhD[3], **James J Pilla, PhD**[1], **Giovanni Ferrari, PhD**[2], **Kevin Koomalsingh, MD**[2], **Mohammed Haris, PhD**[1], **Robin Hinmon**[2], **Gerald Zsido, BA**[1], **Joseph H Gorman III, MD**[2], **Robert C Gorman, MD**[2], and **Ravinder Reddy, PhD**[1]

[1] Center for Magnetic Resonance and Optical Imaging, Department of Radiology, University of Pennsylvania, Philadelphia, PA

[2] Department of Surgery, University of Pennsylvania, Philadelphia, PA

[3] Medical Physics, University Hospital Freiburg, Freiburg im Breisgau, Germany

Abstract

T1ρ relaxation times were quantified in a swine model of chronic, left ventricular myocardial infarction. It was found that there were low frequency relaxation mechanisms that suppress endogenous contrast at low spin lock amplitudes and in T2-weighted images. A moderate amplitude spin locking pulse could overcome these relaxation mechanisms. Relaxation dispersion data was measured over a range of RF field amplitudes and a model was formulated to include dipole-dipole relaxation modulated by molecular rotation and an apparent exchange mechanism. These techniques may find some use in the clinic for the observation of chronic, left ventricular cardiac remodeling.

Introduction

Immediately following myocardial infarction, structural and biochemical changes occur to the heart muscle. Alterations in the size, thickness and geometry of the left ventricle affect patient prognosis through the augmentation of wall stress, impaired systolic contractile function and increased probability of aneurism formation. Chronically, infarct expansion, progressive thinning and deposition of non-contractile fibrotic tissue results in a decreased volume of myocytes together with compensatory dilatation of the noninfarcted remote and border zone segments. Ultimately, cardiac output cannot be sustained under the circumstances of such progressive heart enlargement, resulting in heart failure.

These complex structural and functional changes have a significant influence on the local magnetic environment of the water molecule. In addition, these changes may occur in a time-varying fashion from the moment of initial ischemic insult and throughout the period of dilatation and left ventricular remodeling. Acutely, edematous tissue has been observed to prolong water 1H relaxation times, but the mechanism for 1H relaxation time enhancement is still not well understood. This mechanism might be attributed to a relative increase in the 1H rotational correlation time in the infarcted segment and its modulation through the dipole-dipole interaction, but also the contributions from other possible relaxation mechanisms are not known. Even less well understood, but, however, increasingly more important in the study of left ventricular remodeling, are changes in 1H relaxation times

Corresponding Author: Walter RT Witschey, PhD, Medical Physics, University Hospital Freiburg, 60a Breisacher Str., 79106 Freiburg im Breisgau, Tel: 49-761-270-9378, walter.witschey@uniklinik-freiburg.de.

during chronic ischemia, during which myofibroblasts first deposit and then maintain a network of collagen in the fibrotic infarct region.

T2 relaxation and T2-weighted imaging has been studied in several different fields of heart disease including acute, edematous infarction and chronic infarction (1–5). It was shown that T2 might discriminate early and late infarction on the basis of relaxation time differences and that there were perhaps only small differences which made chronic infarct and remote myocardium indistinguishable (6). In these previous studies, T2 relaxation in cardiac muscle was thought to be caused by changes in the 1H rotational correlation time caused by tissue alteration and edema. There may be, however, other strong contributions to T2 relaxation other than simply changes in the rotational correlation time and may include chemical exchange effects, diffusion through magnetic field gradients, among other mechanisms. These other contributions obscure endogenous contrast between scar, border zone, and healthy tissue, but may be overcome through the use of a moderate spin locking pulse used in a T1rho imaging experiment (7); that is, the spin locking pulse will prevent some relaxation mechanisms from having effect at low frequencies and prolong relaxation times (8,9).

To quantify the origins of molecular spin-spin relaxation in cardiac muscle, we performed a series of T2 and rotating frame, spin-lattice (T1ρ) measurements. Unlike other previous experiments that sought to quantify T2 alone, multiple T1ρ measurements of varying RF field strength provide access to the entire range of low frequency molecular relaxation dispersion. If, indeed, there are additional low frequency relaxation mechanisms between remote, border zone and infarcted myocardium, T1ρ may serve as a potent source of endogenous contrast. For this purpose, we proposed to determine T2 and T1ρ relaxation rate differences in a swine model of chronic myocardial infarction. We measured relaxation times both *in vivo* and *ex vivo* in an isolated segment of cardiac tissue from the same animal and compared these results with standard cardiac histology.

Methods

Animal Model and Care

5 pigs (Yorkshire swine) weighing between 20–25 kg were used in this study. The animal was sedated with IM ketamine (25mg/kg). An endotracheal tube was placed and they were prepped for surgery, which was previously described in an ovine model (10–12). Anesthesia was induced with isoflurane (1–2%). The animal was under complete cardiovascular monitoring. A left thoracotomy was done and the pericardial sac was opened. The left circumflex artery and mid posterior descending artery were ligated to create a 20–25% area of infarction. During MRI the approximate location of the infarct was identified and could be unconditionally confirmed at sacrifice and dissection. After an appropriate period of observation, the chest was closed in layers. The animal was weaned from anesthesia and recovered. After 8 weeks, the animal was returned to the operating room for a terminal study. Arterial and venous access were obtained. A pressure transducer (Millar Instruments, Houston TX) was guided into the left ventricle for cardiac gating. The animal was transported to a MRI scanner and underwent cardiac imaging. At the conclusion of the study animals were euthanized and their hearts excised for further analysis. All animals were treated under experimental protocols approved by the University of Pennsylvania's Institutional Animal Care and Use Committee (IACUC) and in compliance with National Institutes of Health Publication No. 85-23, revised 1996.

In Vivo MRI

Due to arrhythmias secondary to chronic heart failure, only 3 animals survived to the 8-week time point for in vivo MRI. Animals were transported to a 3 T clinical imaging system (Tim Trio Model, Siemens Medical Solutions, Erlangen, Germany) equipped with 40 mT/m nominal gradients, 6 channel spine array receive coil and birdcage body coil. A gradient echo localizer was used to obtain short axis cardiac views. A T1ρ-prepared, centrically segmented, multiecho, gradient echo sequence with Cartesian readout was used to acquire T1ρ-weighted images during systole (13). The parameters used for acquisition were as follows: bandwidth/pixel = 400 Hz, TR = 3500 ms, TE = 3.3 ms, slice thickness = 8 mm, resolution = 2.34 or 1.56 mm^2, matrix = 128 × 128 or 192 × 192, FOV = 300 mm^2, flip angle = 12 degrees, 12 shots, TSL = 12–48 ms in 5 ms increments, scan time = 4.9 minutes, ν_1 = 750 Hz, Tdelay ≈ 190 ms. The spin lock pulse cluster consists of 4 nonselective RF pulses (Figure 1) and was delivered approximately 190 ms after the QRS complex, although this was adjusted to the heart rate of the animal. The first and final pulses are to excite the magnetization into the transverse plane and store it longitudinally for readout. The two spin locking pulses are reversed in phase to correct for heterogeneity in the transmit B1 field by means of a Solomon rotary echo (14,15). The spin lock amplitude was chosen on the basis of the maximum tolerance of the body coil for a 48 ms spin lock pulse. A delay of several seconds was allowed for the restoration of longitudinal magnetization, however, this was also adjusted to the heart rate.

Ex Vivo MRI

For each of the 5 animals, the left ventricle was separated from the heart and a section of tissue with approximate dimensions 80 (circumferential) × 20 (radial) × 10 (longitudinal) mm^3 was cut. The tissue was suspended in a custom-built, tissue imaging device containing saline. Imaging was performed on a 7 T system (Siemens) equipped with 40 mT/m gradients and a custom-built, solenoid coil of 2 cm diameter and interfaced to the scanner with a transmit/receive switch (Stark Contrast, Erlangen, Germany). A T1ρ-prepared fast spin echo sequence was used with the following imaging parameters: bandwidth/pixel = 130 Hz, TR = 3000 ms, $TE_{effective}$ = 15 ms, slice thickness = 1 mm, resolution = 0.23 mm^2, matrix= 256 × 256, FOV = 60 mm^2, echo train length (ETL) = 7, TSL = 10–60 ms in 5 ms increments, scan time = 20 minutes. The spin lock field amplitude was incremented each acquisition (ν_1 = 500, 1000, 1500, 2000, 2500 Hz). An additional T2-prepared(90_x-180_y-90_{-x})fast spin echo was performed with the same imaging parameters as the T1ρ experiment and the measured relaxation times were reported as $\nu_1 = 0$.

Data Analysis

T1ρ relaxation maps were generated by pixelwise, linear, least squares fit. Prior to fitting, each T1ρ-weighted image was smoothed using a Gaussian filter. Each image was noise filtered on the basis of goodness of fit ($\chi^2 \geq 0.1$), maximum and minimum signal intensity, and the appropriateness of T1ρ relaxation times for the cardiac tissues ($0 \leq T1\rho \leq 250$). *In vivo* images were overlaid on T1ρ-weighted images (TSL = 48) and the left ventricle was segmented. Circular regions-of-interest were drawn in the scar and remote myocardium and in the borderzone, which was chosen as a region lying towards the middle of each. The infarct region on the posterior free wall was confirmed at sacrifice and digital photographs of the infarct region were obtained prior to imaging at 7T.

Biochemistry

Tissue sections were fixed in 10% neutral buffered formalin. Five micron sections were obtained for each paraffin embedded block and stained using Masson Trichrome staining.

Collagen stained blue, while muscle, cytoplasm, and keratin stained red. Entire tissue sections were then digitalized using an Aperio scanning microscope (Aperio, Vista, CA).

Statistical Analysis

All statistical analysis was performed in SPSS 16 (SPSS, Inc. IBM; Chicago, IL). 1-Way ANOVA was used to measure relaxation time differences between infarct and remote compartments for each spin lock amplitude *ex vivo* and at 750 Hz *in vivo*. Bonferroni multiple comparisons was used for borderzone and remote compartments, for which differences among relaxation times were small. Dispersion curves were modeled in Matlab (2009b, The MathWorks, Natick, MA) using the nonlinear capabilities (nlinfit).

Results

In this study, a typical set of T1ρ data consisted of a set of T1ρ-weighted images of increasingly greater T1ρ-weighting (Figure 2). The nature of the 1H relaxation times is that, for short TSL times (TSL = 12ms), the image is largely 1H density weighted, with relatively small differences in contrast between tissues. With progressively longer TSL times, the healthy myocardium, which has the shortest relaxation times, relaxes quickly under the influence of the spin locking pulse and appears dark (TSL = 48 ms). Other tissues, such as the infarct region and blood, appear bright on these images because of their longer relaxation times. From a set of these T1ρ-weighted images, a T1ρ map was generated and so the spatial variation of relaxation times is depicted as a colormap. Mean T1ρ varied spatially between the infarct region (T1ρ = 93.3 ± 12.1 ms), borderzone (T1ρ = 59.6 ± 13.0 ms), and remote myocardium (T1ρ = 49.9 ± 6.1 ms ($p < 0.01$). Blood in the left ventricular compartment, which was also visualized in the T1ρ-weighted images, had longer relaxation times (T1ρ = 147.7 ± 21.0), although the effect of RF saturation would tend to make these values relatively shorter than tissue.

Ex vivo imaging was performed to verify that the infarct region corresponded with the infarct scar as it appears by biochemical staining of collagen and cells. There was a near correspondence between the infarct region and prolonged 1H relaxation times (Figure 3). A single, high resolution T1ρ-weighted image can be used to distinguish the collagenous scar from the neighboring myocardial tissue (Figure 3A). The scar is still moderately unrelaxed and appears bright compared to the remote region. A similar T1ρ relaxation map (ν_1 = 2500 Hz) can be used to quantify the 1H relaxation times spatially throughout the scar (T1ρ = 189 ± 26.2) and remote myocardium (T1ρ = 60 ± 2.8) (Figure 3B). The regional transmurality of the infarct can be visualized as well. In this set of images the scar extends only partially through thickness of the myocardial wall. Several features of the T1ρ images (Figures 3A and 3B) have similar appearance to the trichrome stain (Figure 3C) of an adjacent section of tissue, including wall thickness, the appearance of scar at the site of wall thickness narrowing and regional nontransmurality. The location in the left ventricle from which the tissue was segmented is shown in Figure 3D.

Ex vivo 1H relaxation times varied with both the applied spin lock amplitude (ν_1 = 0, 500, 1000, 1500, 2000, 2500; $p < 0.05$) and between infarct, borderzone and remote myocardium ($p < 0.05$) (Figure 4). Moreover, the difference in T1ρ between infarct, borderzone and remote myocardium increased upon increasing the amplitude of the spin lock field ($p<0.05$, Table 1). The increase in relaxation time differences meant that for the same spin lock duration, it was possible to improve the contrast between each of the three regions (Figure 5). A section of tissue containing scar had relaxation times nearly 100 ms longer than in a region of healthy myocytes, at the highest spin lock amplitude ($\nu1$ = 2500 Hz). The relative increase in relaxation time per unit of applied RF, however, was less for higher spin lock

amplitudes, suggesting that low frequency dispersion may have approached an asymptotic value by 2500 Hz.

To explore possible mechanisms for T1ρ relaxation, the apparent exchange correlation time was quantified using the single Lorentzian model derived in Appendix A (Table 2). Although this model is somewhat simpler than those previously used, it was appropriate for the small number of RF field strengths for which relaxation times were measured. The relaxation rate was expressed as a sum over contributions from individual relaxation mechanisms and the fitted model is shown in Figure 6. The apparent exchange rate increased in the remote and borderzone regions compared to the infarct region. A decrease in the apparent exchange rate shifts the R1ρ dispersion to the left and this could be used as a source of contrast. The differences in tissue relaxation on account of dipole-dipole relaxation, however, are the primary mechanism for contrast differences between the tissues at RF field amplitudes above 400 Hz.

Discussion

It was found that there exist relaxation mechanisms that operate below approximately 500 Hz, which suppress endogenous contrast between myocardial tissues, healthy myocytes and mature scar, 8 weeks following a myocardial infarction. By delivering a spin locking pulse of sufficient power, it is possible to overcome these relaxation mechanisms and reveal much greater differences in relaxation times than could be achieved with a similar T2 experiment. Between 0 and 2.5 kHz, relaxation was interpreted using a two-site exchange model, which assumed that there were two such contributions to the overall relaxation rate: (1) the dipole-dipole interaction modulated by rotational motion of the ^{1}H nuclei and (2) nuclear exchange between two sites with different chemical shifts in a manner consistent with previous models of T1ρ relaxation in biological tissues (16–23).

In complex biological tissues this model can be considered only a very rough approximation of true events, which consist of numerous exchangeable sites on a multitude of different proteins and molecules, and the existence of magnetic field gradients through which nuclei are constantly diffusing. For these reasons, it is not clear over this range of frequencies whether such a model can distinguish between real differences in the apparent exchange rate measured in Table 2. Nevertheless, the asymptotic value of the relaxation rate over this range, which represents the contribution from dipole-dipole relaxation modulated by rotational motion, is clearly different. This suggests, at the very least, that water 1H nuclei in myocardial scar tissue are more mobile than those in healthy myocytes, dependent or not on the relative water content in each tissue type. These findings may quite generally apply to any collagenous scar tissue.

T1ρ was quantified here in the case of chronic myocardial infarction, however, it has also been used to quantify differences in contrast and signal-to-noise ratio in several patients following acute myocardial infarction (24,25). It should be understood that both the nature of the disease and the focus of the experiment were different in these previous cases. In the acute case, it was suggested that following myocardial apoptosis and cell death, there is a leakage of protein material from the sarcolemma into the surrounding extracellular space, minimizing the effect of proteins on water molecules. Whether the relaxation time enhancement in the case of edema was because of the increase in the 1H water rotational correlation time, a chemical exchange mechanism, or some combination thereof, is unclear. For example, the contribution from magnetization transfer of the type between a free water pool and a separate pool in close proximity to macromolecules is modeled only indirectly through the apparent exchange rate in the present study. Still, many more questions remain

concerning the molecular mechanisms for T1ρ relaxation during acute myocardial infarction.

It is worth discussing in some detail the design of T1ρ pulse sequences used for imaging the heart. There are some differences between the previously used pulse sequence (24–26) and that which was used in the present context. The spin lock amplitude used in those experiment was considerably weaker (v1 = 123 Hz for an 8 ms, 360 degree pulse) than in the present experiments, such that the relaxation time differences between T2 and T1ρ in edemic tissues and healthy tissues may have been much different if measured using the in vivo field strength measured here (v_1 = 750 Hz). However, the effect on the contrast cannot be so easily determined, because a hybrid T1ρ cine sequence would excite, lock and store the magnetization repeatedly over the course of a single heart beat. If longitudinal relaxation were not allowed to occur, for instance, by acquiring data every heart beat, the sequence would build up a steady-state that was a complicated function of the cine segment size, the duration and amplitude of the spin lock field and the heart rate itself.

In the present experiment, no cine imaging was performed so that a single T1ρ map could be obtained during systole and that the corresponding equation for relaxation could be described with a single exponential model. This has some disadvantages in that the motion of the heart must be obtained using a separate cine acquisition, fortunately however, usually short. The motion of the heart, particularly the thickening of the myocardial wall, may have some effect on transverse relaxation times by reducing the rotational correlation time. For this reason, a spin lock experiment may be able to distinguish diastolic from systolic water relaxation times and provide a surrogate measure of regional myocardial contractility.

The spin lock amplitudes typically used for ex vivo imaging were not possible to achieve in vivo. The strength of the spin lock field is limited both by the capabilities of the hardware and the specific absorption rate of radiation (SAR) delivered to tissues. At 3T, the field strength of a 48 ms pulse was limited by the capabilities of the body coil, and likely, field strengths on the order of 400 Hz are more appropriate for conditions in which the load on the body coil changes, such as during patient scanning. Under variable conditions, the power required to lock the spins can vary from person to person. For ideal conditions, it is suitable to use an even longer duration locking pulse, so that the transverse magnetization in the remote myocardium is more fully relaxed with respect to the infarct, thereby improving contrast. When the duration of the locking pulse becomes much longer than the durations used here, for example, on the order of 100 ms, it is necessary to divide the locking pulse up into individual pulses of shorter duration and perhaps also reduce the RF amplitude. The consequence is that there must always be some balance between the length of the interpulse delay and the lock durations and amplitudes used.

The results from such a small number of animals (3) scanned *in vivo* should be interpreted with some care, especially compounded with possible sources of error including changes in myocardial wall thickness and stress, B1 and B0 heterogeneity, as well as partial volume effects. However, because of these promising preliminary results, we have undertaken a plan for future studies that will encompass many animals followed over a period from baseline and initial onset of infarction to chronic infarction. The results of this future study will enable robust assessment of group characteristics of edema and the formation of scar and their influence onMR properties of ^{1}H nuclei. Nevertheless, unlike scans of patients with ischemic cardiomyopathies, the target area for infarction in these swine was well-defined during surgery, having been restricted to the left circumflex artery and mid posterior descending artery to create an infarction approximately 20–25% the size of the left ventricular and constrained to the outer free wall apposed the lung. During MRI the approximate location of the infarct was identified and could be unconditionally confirmed at

sacrifice and dissection. *Ex vivo*, samples of cardiac tissue from six different animals were visually confirmed to contain infarcted, borderzone and healthy myocardium. Consequently, the location of the infarct was unambiguous and validates the results of measured relaxation times.

From these experiments, it's clear that by increasing the spin lock amplitude, one can maximize the relaxation time differences between infarct, border zone, and remote myocardium, however, one also can overcome the significant B0 homogeneity in the cardiothoracic cavity. The air-filled lung together with cardiac and respiratory motion can have a considerable, deleterious effect on B0 field homogeneity in the chest. This problem was compounded in the present situation through the use of a left ventricular pressure transducer used for cardiac gating. Oftentimes, the pressure transducer would coil in the left ventricle, even when care was taken to avoid such an event from occurring. At low spin lock amplitudes, nutation about a tilted effective field can result in image artifacts. In further experiments, we plan to make use of an integrated spin echo and spin lock approach to somewhat compensate for both B1 andB0 fields (27)although a pulse sequence had not yet been prepared for these experiments. Problems related to B1 homogeneity were reduced through the Solomon rotary echo, although variations in the RF field in the cardiothoracic cavity often occur at 3 T.

The biochemistry of the tissue has a strong effect on the 1H relaxation times, but these changes are obscured by the poor scanning resolution *in vivo* through partial volume effects. While the scar tissue consists predominantly of collagen and extracellular martrix components, the neighboring borderzone consists of myocytes and extracellular matrix material, but also bundles of collagen fibers that anchor the scar to the surrounding healthy muscle. Consequently, a voxel in the borderzone region consists of a partial volume of bundles of collagen fibers and myocytes. If 1H proximal to collagen bundles has similar relaxation times to scar tissue, then there would be a tendency for relaxation times in the borderzone to be average of 1H relaxation times in the scar and healthy myocytes.

Conclusion

In this T1ρ dispersion study of chronic myocardial infarction in swine, it was discovered that there are mechanisms for spin-spin relaxation that operate at low frequency below 1 kHz. These relaxation mechanisms obscure endogenous contrast between healthy myocytes and collagenous scar in cardiac tissue. By applying a moderate amplitude spin locking pulse, it is possible to overcome these mechanisms of relaxation and enhance relaxation time differences in these tissues. The study of relaxation mechanisms in the heart is not well understood, but the advantages of spin locking may have some important applications in the clinic.

Acknowledgments

We would like to thank support from the National Institutes of Health grants RR02305, AR45404, HL63954, HL73021, and HL76560 and the German Federal Ministry of Education and Research grant 13N9208.

References

1. Miller S, Helber U, Kramer U, Hahn U, Carr J, Stauder NI, Hoffmeister HM, Claussen CD. Subacute myocardial infarction: assessment by STIR T2-weighted MR imaging in comparison to regional function. MAGMA. 2001; 13(1):8–14. [PubMed: 11410391]
2. Simonetti OP, Finn JP, White RD, Laub G, Henry DA. "Black blood" T2-weighted inversion-recovery MR imaging of the heart. Radiology. 1996; 199(1):49–57. [PubMed: 8633172]

3. Higgins CB, Herfkens R, Lipton MJ, Sievers R, Sheldon P, Kaufman L, Crooks LE. Nuclear magnetic resonance imaging of acute myocardial infarction in dogs: alterations in magnetic relaxation times. Am J Cardiol. 1983; 52(1):184–188. [PubMed: 6858909]
4. Boxt LM, Hsu D, Katz J, Detweiler P, McLaughlin S, Kolb TJ, Spotnitz HM. Estimation of myocardial water content using transverse relaxation time from dual spin-echo magnetic resonance imaging. Magn Reson Imaging. 1993; 11(3):375–383. [PubMed: 8505871]
5. Scholz TD, Fisher DJ, Ehrhardt JC, Skorton DJ. Interventricular differences in myocardial T2 measurements: experimental and clinical studies. J Magn Reson Imaging. 1991; 1(5):513–520. [PubMed: 1790375]
6. Abdel-Aty H, Zagrosek A, Schulz-Menger J, Taylor AJ, Messroghli D, Kumar A, Gross M, Dietz R, Friedrich MG. Delayed enhancement and T2-weighted cardiovascular magnetic resonance imaging differentiate acute from chronic myocardial infarction. Circulation. 2004; 109(20):2411–2416. [PubMed: 15123531]
7. Sepponen RE, Pohjonen JA, Sipponen JT, Tanttu JI. A method for T1 rho imaging. J Comput Assist Tomogr. 1985; 9(6):1007–1011. [PubMed: 4056129]
8. Slichter CP, Ailion D. Low-Field Relaxation and the Study of Ultraslow Atomic Motionsby Magnetic Resonance. Phys Rev. 1964; 135:A1099.
9. Desvaux H, Berthault P. Study of dynamic processes in liquids using off-resonance rf irradiation. Prog Nuc Mag Res Sp. 1999; 35(4):295–340.
10. Blom AS, Pilla JJ, Arkles J, Dougherty L, Ryan LP, Gorman JH 3rd, Acker MA, Gorman RC. Ventricular restraint prevents infarct expansion and improves borderzone function after myocardial infarction: a study using magnetic resonance imaging, three-dimensional surface modeling, and myocardial tagging. Ann Thorac Surg. 2007; 84(6):2004–2010. [PubMed: 18036925]
11. Pilla JJ, Blom AS, Gorman JH 3rd, Brockman DJ, Affuso J, Parish LM, Sakamoto H, Jackson BM, Acker MA, Gorman RC. Early postinfarction ventricular restraint improves borderzone wall thickening dynamics during remodeling. Ann Thorac Surg. 2005; 80(6):2257–2262. [PubMed: 16305885]
12. Blom AS, Mukherjee R, Pilla JJ, Lowry AS, Yarbrough WM, Mingoia JT, Hendrick JW, Stroud RE, McLean JE, Affuso J, Gorman RC, Gorman JH 3rd, Acker MA, Spinale FG. Cardiac support device modifies left ventricular geometry and myocardial structure after myocardial infarction. Circulation. 2005; 112(9):1274–1283. [PubMed: 16129812]
13. Witschey WR, Borthakur A, Elliott MA, Fenty M, Sochor MA, Wang C, Reddy R. T1rho-prepared balanced gradient echo for rapid 3D T1rho MRI. J Magn Reson Imaging. 2008; 28(3):744–754. [PubMed: 18777535]
14. Solomon I. Rotary Spin Echoes. Phys Rev Lett. 1959; 2:301.
15. Charagundla SR, Borthakur A, Leigh JS, Reddy R. Artifacts in T(1rho)-weighted imaging: correction with a self-compensating spin-locking pulse. J Magn Reson. 2003; 162(1):113–121. [PubMed: 12762988]
16. Jokivarsi KT, Niskanen JP, Michaeli S, Grohn HI, Garwood M, Kauppinen RA, Grohn OH. Quantitative assessment of water pools by T 1 rho and T 2 rho MRI in acute cerebral ischemia of the rat. J Cereb Blood Flow Metab. 2009; 29(1):206–216. [PubMed: 18827834]
17. Sierra A, Michaeli S, Niskanen JP, Valonen PK, Grohn HI, Yla-Herttuala S, Garwood M, Grohn OH. Water spin dynamics during apoptotic cell death in glioma gene therapy probed by T1rho and T2rho. Magn Reson Med. 2008; 59(6):1311–1319. [PubMed: 18506797]
18. Duvvuri U, Goldberg AD, Kranz JK, Hoang L, Reddy R, Wehrli FW, Wand AJ, Englander SW, Leigh JS. Water magnetic relaxation dispersion in biological systems: the contribution of proton exchange and implications for the noninvasive detection of cartilage degradation. Proc Natl Acad Sci USA. 2001; 98(22):12479–12484. [PubMed: 11606754]
19. Michaeli S, Sorce DJ, Springer CS Jr, Ugurbil K, Garwood M. T1rho MRI contrast in the human brain: modulation of the longitudinal rotating frame relaxation shutter-speed during an adiabatic RF pulse. J Magn Reson. 2006; 181(1):135–147. [PubMed: 16675277]
20. Grohn OHJ, Kettunen MI, Makela HI, Penttonen M, Pitkanen A, Lukkarinen JA, Kauppinen RA. Early detection of irreversible cerebral ischemia in the rat using dispersion of the magnetic

resonance imaging relaxation time, T1rho. J Cereb Blood Flow Metab. 2000; 20(10):1457–1466. [PubMed: 11043908]

21. Kettunen MI, Grohn OH, Penttonen M, Kauppinen RA. Cerebral T1rho relaxation time increases immediately upon global ischemia in the rat independently of blood glucose and anoxic depolarization. Magn Reson Med. 2001; 46(3):565–572. [PubMed: 11550250]
22. Kettunen MI, Grohn OH, Silvennoinen MJ, Penttonen M, Kauppinen RA. Effects of intracellular pH, blood, and tissue oxygen tension on T1rho relaxation in rat brain. Magn Reson Med. 2002; 48(3):470–477. [PubMed: 12210911]
23. Grohn OH, Lukkarinen JA, Silvennoinen MJ, Pitkanen A, van Zijl PC, Kauppinen RA. Quantitative magnetic resonance imaging assessment of cerebral ischemia in rat using on-resonance T(1) in the rotating frame. Magn Reson Med. 1999; 42(2):268–276. [PubMed: 10440951]
24. Huber S, Muthupillai R, Lambert B, Pereyra M, Napoli A, Flamm SD. Tissue characterization of myocardial infarction using T1rho: influence of contrast dose and time of imaging after contrast administration. J Magn Reson Imaging. 2006; 24(5):1040–1046. [PubMed: 16972231]
25. Muthupillai R, Flamm SD, Wilson JM, Pettigrew RI, Dixon WT. Acute myocardial infarction: tissue characterization with T1rho-weighted MR imaging--initial experience. Radiology. 2004; 232(2):606–610. [PubMed: 15215547]
26. Dixon WT, Oshinski JN, Trudeau JD, Arnold BC, Pettigrew RI. Myocardial suppression in vivo by spin locking with composite pulses. Magn Reson Med. 1996; 36(1):90–94. [PubMed: 8795026]
27. Witschey WR 2nd, Borthakur A, Elliott MA, Mellon E, Niyogi S, Wallman DJ, Wang C, Reddy R. Artifacts in T1 rho-weighted imaging: compensation for B(1) and B(0) field imperfections. J Magn Reson. 2007; 186(1):75–85. [PubMed: 17291799]
28. Michaeli S, Sorce DJ, Idiyatullin D, Ugurbil K, Garwood M. Transverse relaxation in the rotating frame induced by chemical exchange. J Magn Reson. 2004; 169(2):293–299. [PubMed: 15261625]
29. Fischer MWF, Majumdar A, Zuiderweg ERP. Protein NMR relaxation: theory, applications and outlook. Prog Nuc Mag Res Sp. 1998; 33(3–4):207–272.
30. Davis DG, Perlman ME, London RE. Direct measurements of the dissociation-rate constant for inhibitor-enzyme complexes via the T1 rho and T2 (CPMG) methods. J Magn Reson B. 1994; 104(3):266–275. [PubMed: 8069484]

Appendix

Model for T1ρ Dispersion

The dispersion of the spin lattice (T1) relaxation time with B_0 field strength may be used to examine molecular dynamics, however, in several cases, rotating frame, spin lattice (T1ρ) has been used as an alternative method *in vivo*. T1ρ is particularly useful when the range for which relaxation dispersion occurs is at very low frequency (Hz-KHz), because a similar T1 experiment would significantly reduce the observable spin signal. There are several possible mechanisms for *in vivo* T1 ρ dispersion, which were considered in the present model and this treatment is similar to that which has been pursued in (23,28).

Dipole-Dipole Relaxation

Magnetic field fluctuations at the site of a 1H nucleus that originate from other identical nuclei are responsible for dipole-dipole relaxation. During a spin locking pulse, the contribution to the nuclear relaxation rate is

$$R_{1\rho,dd}=\frac{1}{10k_{dd}}\left\lfloor\frac{3}{1+4\omega_1^2\tau_c^2}+\frac{5}{1+\omega_0^2\tau_c^2}+\frac{2}{1+4\omega_0^2\tau_c^2}\right\rfloor \quad [1]$$

and

$$\frac{1}{k_{dd}}=2I(I+1)\hbar^2\gamma^4 r^{-6}\tau_c \quad [2]$$

Here the spin angular momentum quantum number $I=\frac{1}{2}$, h is Planck's constant and r (1.58 Å) is the internuclear distance. For a system in which ^{1}Hs are in two-site chemical exchange (2SX), each site (A and B) has a contribution to the relaxation time ($R_{1\rho A}$ and $R_{1\rho B}$). From Equation [1], it can be seen that changes in the relaxation rate will occur if either the Larmor frequency ω_0 or the RF field amplitude ω_1 coincides with the rotational correlation time τ_c.

Chemical Exchange

Chemical exchange between ^{1}H sites separated by a chemical shift difference $\delta\omega$ may also cause 1. In particular, for two-site chemical exchange in the fast exchange regime, the relaxation rate is (29,30)

$$R_{1\rho,ex}=\frac{P_A P_B \delta\omega^2 \tau_{ex}}{1+\omega_1^2\tau_{ex}^2} \quad [3]$$

where P_A and P_B are the fractional populations of the spin pools and the exchange time $\tau_{ex}=\frac{1}{k_{ex}}$.

Dispersion Model

In several *in vivo* studies, the relaxation dispersion was modeled as sum of contributions from the dipole-dipole and chemical exchange relaxation rates.

$$R_{1\rho}=P_A R_{1\rho,dd,A}+P_B R_{1\rho,dd,B}+R_{1\rho,ex} \quad [4]$$

For two site chemical exchange, site *A* represents the free water fraction, which resonates with the RF field and has a rotational correlation time on the order of picoseconds. Site *B* represents a bound water fraction of unknown size with a single chemical shift ($\delta\omega \ll 2$ *KHz*). The fractional size of the pools $P_A + P_B = 1$.

On account of the limited range over which dispersion was measured (0–2.5 kHz), the contribution to the dipole-dipole relaxation rate was treated as approximately constant. Certainly, for the case of the free water fraction $\omega_1\tau_{c,A} \ll 1$, this is appropriate. Although, the rotational correlation time for site B is unknown, here, it is assumed also that $\omega_1\tau_{c,B} \ll 1$, so that

$$R_{1\rho}=\frac{A\tau_{ex}}{1+\omega_1^2\tau_{ex}^2}+B \quad [5]$$

where $A = P_A P_B \delta\omega^2$.

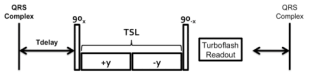

Figure 1.
Pulse sequence used for T1ρ-weighted imaging. The spin locking pulse cluster was delivered approximately 190 ms from the QRS complex in systole. Triggering was achieved using a pressure transducer in the left ventricle. Following the pulse cluster, the T1 ρ-prepared magnetization was acquired for imaging using a multiecho gradient echo sequence. Following image acquisition, a period of several seconds was allowed for regrowth of longitudinal magnetization.

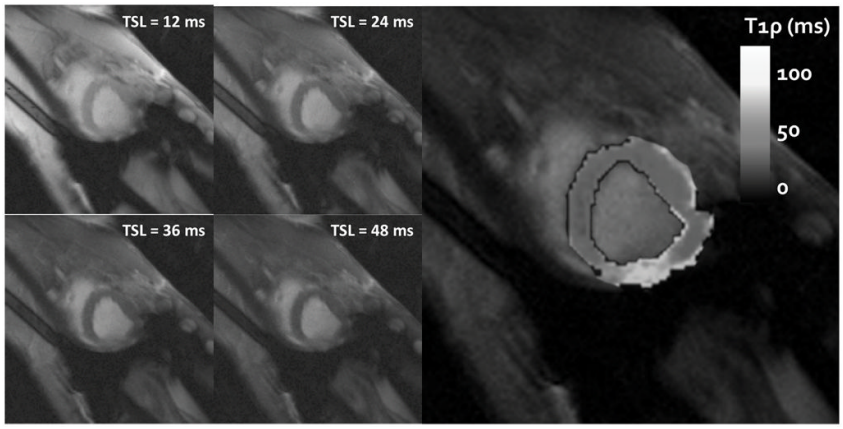

Figure 2.

Four T1ρ-weighted images at different spin lock durations (TSL = 12–48 ms) are shown on the left demonstrating the relaxation dependent contrast in the left ventricular wall. The infarct region on the left ventricular free wall has longer relaxation times and appears bright next to the healthy myocardial wall. A relaxation map (ν1 = 750 Hz) is shown on the right and shows enhanced relaxation times in the free wall region.

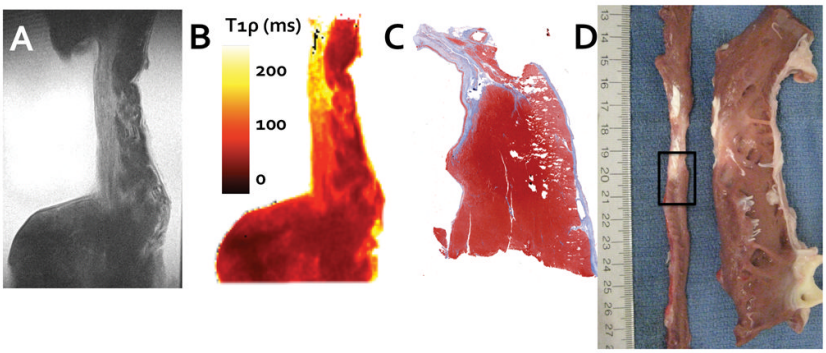

Figure 3.

To confirm the T1ρ relaxation time enhancement, tissue was excised from the left ventricular wall and scanned at high resolution. A single T1ρ-weighted image (A, TSL = 48 ms) is shown alongside the corresponding T1ρ relaxation map (B) and shows relaxation time enhancement in the thin region of the left ventricular wall. This relaxation time enhancement corresponds with the collagenous scar identified by trichrome biochemical staining (C) and digital photographs of the same region immediately after sacrifice (D). In (D), the left ventricle has been sliced along the vertical long axis, unwrapped, and sliced again along the short axis (narrow thin strip of tissue on the left). The interface between infarct and borderzone tissue identified for ex vivo imaging is outlined (black rectangle).

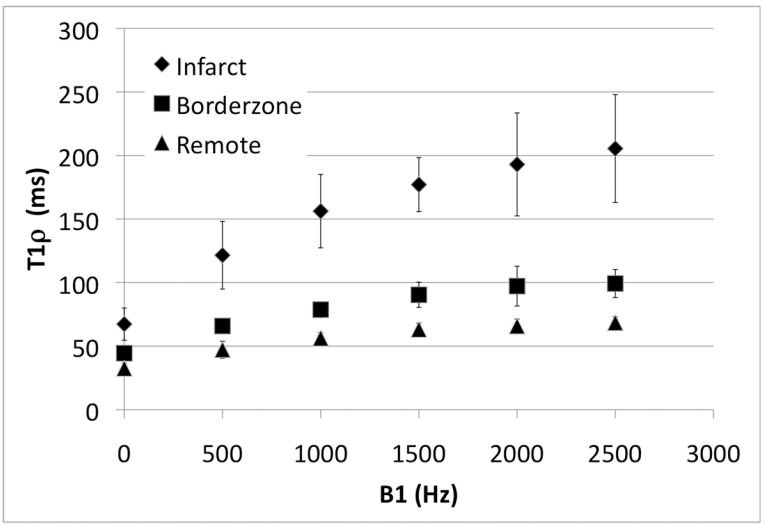

Figure 4.

The variation in T1ρ relaxation times with RF field amplitude (T1ρ dispersion) for each region (infarct, borderzone and remote regions of myocardium) is shown. The relaxation rate difference between tissue types increases with RF field strength, thereby enhancing contrast in T1ρ-weighted images.

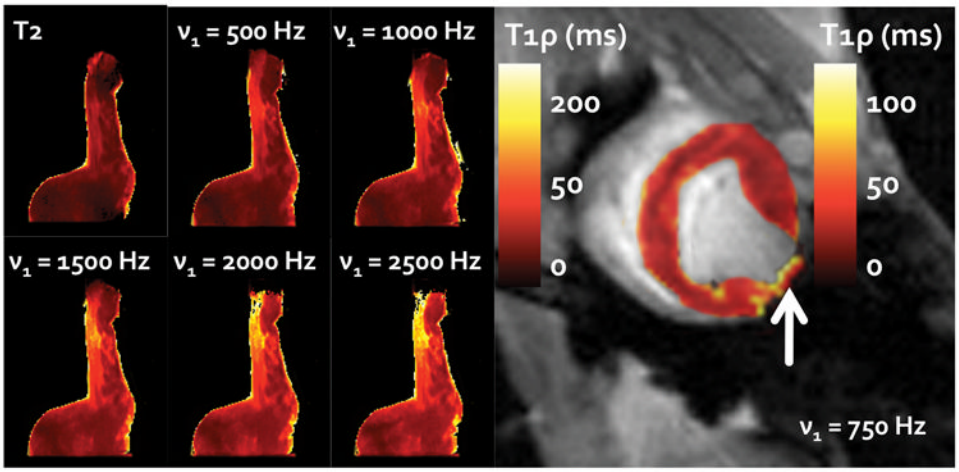

Figure 5.

The six images on the left demonstrate the change in relaxation times and relative enhancement of contrast through the use of an increasingly greater RF spin lock field (v_1 = 500–2500 Hz, B_0 = 7T). These images are shown alongside a comparable T2 relaxation map of the same slice. A corresponding left ventricular *in vivo* T1ρ-relaxation map is shown on the right (v_1 = 750 Hz, B_0 = 3T). The arrow depicts the infarct area on the free wall. Note that the scales for the *ex vivo* and *in vivo* images are different.

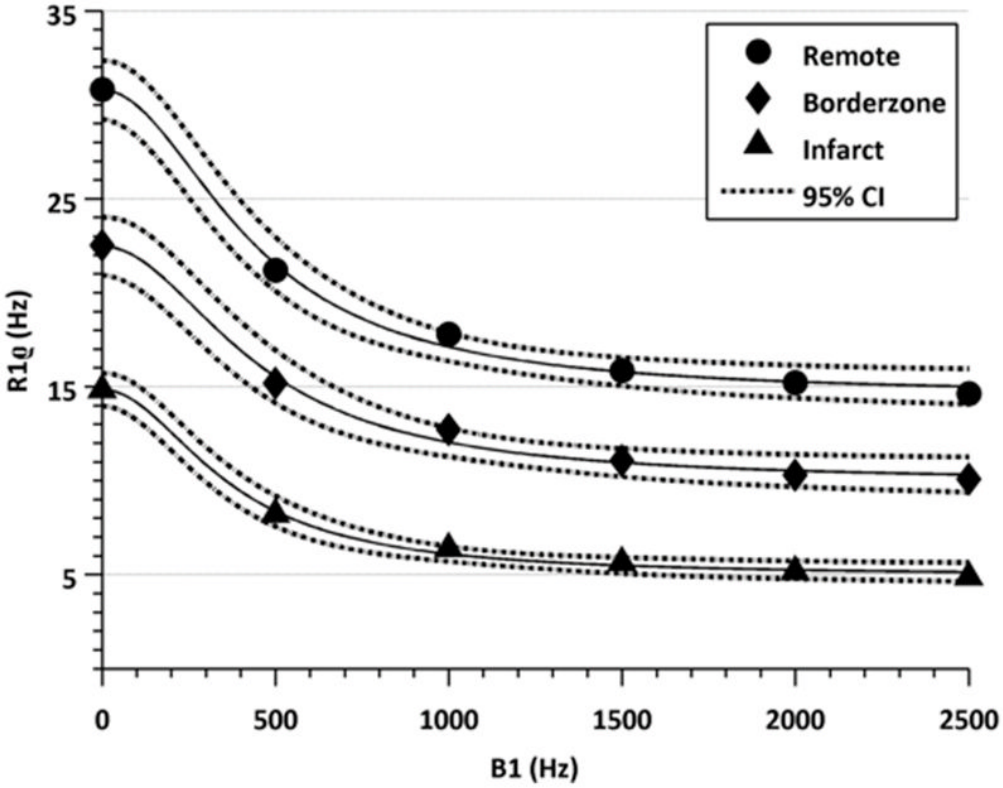

Figure 6.
The variation in the relaxation rate with RF field strength and corresponding best fit to Eq. 4. The model encompasses both dipole-dipole relaxation and apparent chemical exchange rate and was used for quantification of $R1_{dd}$ and k_{ex} in Table 2.

Table 1

	Relaxation Time Differences by Region					
	ΔT2 (ms) **ΔR2 (s^{-1})**	**ΔT1ρ (ν_1 = 500 Hz) (ms)** **ΔR1ρ(s^{-1})**	**ΔT1ρ (ν_1 = 1000 Hz) (ms)** **ΔR1ρ(s^{-1})**	**ΔT1ρ (ν_1 = 1500 Hz) (ms)** **ΔR1ρ(s^{-1})**	**ΔT1ρ (ν_1 = 2000 Hz) (ms)** **ΔR1ρ(s^{-1})**	**ΔT1ρ (ν_1 = 2500 Hz) (ms)** **ΔR1ρ(s^{-1})**
Infarct/Remote*	34.9 28.7	74.3 13.5	99.9 10.0	114.0 8.7	127.2 7.9	137.1 7.3
Confidence Interval (95%) [L U]†	[20.3 49.4]	[41.1 107.6]	[69.6 130.0]	[89.6 138.4]	[82.8 171.6]	[92.2 181.8]
Infarct/Borderzone*	22.9 43.7	55.7 18.0	77.5 12.9	86.7 11.5	95.8 10.4	106.1 9.4
Confidence Interval (95%) [L U]	[8.4 37.4]	[22.4 89.0]	[47.2 107.8]	[62.3 111.1]	[51.4 140.2]	[61.4 151.0]
Borderzone/Remote**	11.9 84.0	18.6 53.8	22.4 44.6	27.2 36.8	31.4 31.8	30.9 32.4

*$p < 0.00$ for each ν_1 (One-Way ANOVA)

**$p < 0.05$ for all ν_1 (Bonferonni Multiple Comparisons)

†Confidence interval is reported for ΔT2 and ΔT1ρ

Table 2

	$R1\rho_{dd}$ (Hz)	k_{ex} (Hz)	$P_aP_b\Delta\omega^2$ $(Hz)^2$
Border	9.9 [8.8 11.0]	4.5 * 10^2 [3.4 6.6]	5.6 [3.7 7.6] × 10^3
Remote	14.5 [13.4 15.6]	4.3 * 10^2 [3.4 5.5]	7.1 [5.1 9.0] × 10^3
Infarct	4.9 [4.4 5.5]	3.7 * 10^2 [2.9 4.7]	3.6 [2.6 4.6] × 10^3

* [L U] denotes the 95 % confidence interval